

# Improved stability due to local pressure flattening in stellarators

K. Ichiguchi

National Institute for Fusion Science,  
Oroshi, Toki, Japan

M. Wakatani, T. Unemura

Graduate School of Energy Science, Kyoto University,  
Gokasho, Uji, Japan

T. Tatsuno

Graduate School of Frontier Science, University of Tokyo,  
Tokyo, Japan

B.A. Carreras

Oak Ridge National Laboratory,  
Oak Ridge, Tennessee, United States of America

**Abstract.** It is demonstrated that the stability of low  $n$  pressure gradient driven modes in stellarators is improved by local flattening of the pressure at low order rational surfaces. Here  $n$  is the toroidal mode number. Results are presented for the Large Helical Device with an inward magnetic axis shift of 25 cm.

## 1. Introduction

The largest stellarator/heliotron device, the Large Helical Device (LHD), has successfully started physics experiments [1]. The electron and ion temperatures  $T_e \approx 3.8$  keV and  $T_i \approx 2.8$  keV were obtained in the low density range  $\bar{n}_e \approx 1.5 \times 10^{19} \text{ m}^{-3}$  [2]. The energy confinement time obtained was about 50% better than the International Stellarator Scaling of energy confinement [3]. The maximum average beta value,  $\bar{\beta} \simeq 2.4\%$ , exceeded 2%, which was the highest beta obtained in stellarator/heliotron devices [4]. Because  $\bar{\beta} \simeq 2.4\%$  is not limited by MHD instabilities and the target beta value of LHD is 5%, a higher power heating is expected in an optimized magnetic configuration.

In this paper we will discuss the effects of local pressure profile flattening on interchange modes which may affect the stability and confinement properties of LHD. For studying MHD stability in stellarator/heliotron devices, the Mercier criterion [5] is valuable. For three dimensional MHD equilibria under the assumption of the existence of flux surfaces, the Mercier criterion is usable for evaluating the beta limit [6]. Another important ingredient of three dimensional MHD equilibrium and stability is the formation of magnetic islands [7]. This is related to the existence of three dimensional nested flux

surfaces [8]. The magnetic islands may be produced by resonant perturbed magnetic fields which are generated by internal resistive MHD instabilities or external error fields. If the magnetic islands appear at low order rational surfaces, it is expected that the pressure profile will become flat in the island regions. It is shown that the MHD stability based on the Mercier criterion changes significantly, although the pressure flattening is highly localized in the neighbourhood of the relevant rational surfaces [9–11]. For this situation the stability limit to the low mode number interchange modes is the important criterion.

In Section 2, reduced MHD equations and a model for describing a pressure profile with locally flat regions at rational surfaces are given. In Section 3, improvement of the stability limit is discussed briefly for cylindrical model stellarators. In Section 4, the relation between the width of local pressure flattening and the growth rates of interchange modes is shown for the LHD case in the toroidal model. Examples of pressure profiles to suppress the low  $n$  mode are also shown. In Section 5, we summarize our results and discuss how they allow reinterpretation of the analysis of the high  $\beta$  CHS and LHD experiments that seem to violate the Mercier criterion when evaluated using smooth pressure profiles.

## 2. Reduced MHD equations and a model pressure profile with locally flat regions at rational surfaces

For analysing pressure driven instabilities in stellarator/heliotron devices, we use the ideal reduced MHD equations [6, 10, 12], which are written as

$$\frac{\partial \psi}{\partial t} = -(R/R_0)^2 \mathbf{B} \cdot \nabla u \quad (1)$$

$$\rho \frac{d}{dt} \nabla_{\perp}^2 u = -\mathbf{B} \cdot \nabla (\nabla_{\perp}^2 \psi) + R_0^2 \nabla \Omega \times \nabla P \cdot \nabla \zeta \quad (2)$$

$$\frac{dP}{dt} = 0 \quad (3)$$

where

$$\mathbf{B} \cdot \nabla = \frac{R_0 B_0}{R^2} \frac{\partial}{\partial \zeta} - \nabla \psi \times \nabla \zeta \cdot \nabla_{\perp} \quad (4)$$

$$\frac{d}{dt} = \frac{\partial}{\partial t} + (R/R_0)^2 \nabla u \times \nabla \zeta \cdot \nabla_{\perp} \quad (5)$$

$$\Omega = \frac{1}{2\pi} \int_0^{2\pi} d\zeta \left( \frac{R}{R_0} \right)^2 \left( 1 + \frac{|\mathbf{B} - \overline{\mathbf{B}}|^2}{B_0^2} \right) \quad (6)$$

$$\nabla_{\perp} = \nabla - \nabla \zeta (\partial / \partial \zeta). \quad (7)$$

Here  $\psi$ ,  $u$  and  $P$  denote the poloidal flux function, the stream function and the plasma pressure, respectively. The axisymmetric component of the magnetic field is given by  $\overline{\mathbf{B}}$ , and  $R$  and  $\zeta$  denote the major radius and the toroidal angle, respectively. The magnetic axis is  $R = R_0$ , and the toroidal field at  $R = R_0$  is  $B_0$ . Because the free boundary effect is not significant for the stability of currentless plasmas, a perfectly conducting wall is usually placed at the plasma boundary [10]. Note that the equilibrium state of  $\psi$  is consistent with the rotational profile due to stellarator fields.

For describing the locally flat pressure profile,

$$P(\rho) = C[P_0(\rho) + P_{ax}(\rho) + P_{res}(\rho) - A] \quad (8)$$

is assumed, where  $P_0(\rho)$  denotes a standard smooth pressure profile,  $P_{ax}(\rho)$  corresponds to a flattening of pressure profile near the magnetic axis given by

$$P_{ax}(\rho) = [P_0(0) - P_0(\rho)] \exp \left[ -\frac{1}{2} \left( \frac{\rho}{w_a} \right)^4 \right] \quad (9)$$

and  $P_{res}(\rho)$  plays a role in flattening the pressure at rational surfaces

$$P_{res}(\rho) = \sum_m \{ [P_0(\rho_m) + P_{ax}(\rho_m)] - [P_0(\rho) + P_{ax}(\rho)] \} \times \exp \left[ -\frac{1}{2} \left( \frac{\rho - \rho_m}{w_m} \right)^4 \right]. \quad (10)$$

Here  $\rho$  denotes the square root of normalized toroidal flux. In Eq. (8),  $A$  and  $C$  are numerical factors to fix pressures at both the magnetic axis and the plasma surface. In Eq. (9),  $w_a$  denotes the width of a region of flat pressure profile near the magnetic axis. In Eq. (10),  $\rho_m$  denotes the position of the  $m$ -th rational surface and  $w_m$  denotes the width of a region of flat pressure profile at the rational surface  $\rho = \rho_m$ .

To calculate fixed boundary MHD equilibria for the LHD configuration with the pressure shown by Eq. (8), the VMEC code [13] was applied. In the following calculations the LHD configuration with an inward magnetic axis shift of 25 cm is considered. Ideal MHD stability against pressure driven modes was studied with the RESORM code [14], which solves the linearized Eqs (1)–(3) as an initial value problem.

## 3. Predictions based on a cylindrical stellarator model for stability of interchange modes in locally flattened pressure profiles at rational surfaces

For studying the beta limit due to interchange modes, the linearized reduced MHD equations are solved for assumed cylindrical stellarator/heliotron plasmas; the equations are reduced to [9]

$$\gamma^2 \nabla_{\perp}^2 u = -(n - m\iota) \nabla_{\perp}^2 [(n - m\iota)u] - D_s \frac{m^2}{r^2} u \quad (11)$$

where  $D_s$  and the averaged helical curvature  $\Omega$  are expressed as

$$D_s = -\frac{\beta_0}{2\epsilon^2} P' \Omega' \quad (12)$$

$$\Omega = \epsilon^2 N \left( r^2 \iota + 2 \int r \iota dr \right). \quad (13)$$

Here  $\epsilon = a/R_0$  denotes the inverse aspect ratio,  $\beta_0 = 2\mu_0 P_0(r = 0)/B_0^2$  the central plasma beta

value and  $N$  the toroidal period number of the helical field. The polarity of the helical field is assumed as  $L = 2$  in Eq. (12). In order to derive Eq. (11), all perturbed quantities are assumed to be proportional to  $\exp[\gamma t - i(m\theta - n\zeta)]$ . In Eq. (11), the prime denotes the derivative with respect to the normalized minor radius  $r$ . The perpendicular Laplacian operator in Eq. (10) is expressed as

$$\nabla_{\perp}^2 = \frac{1}{r} \frac{d}{dr} \left( r \frac{d}{dr} \right) - \frac{m^2}{r^2}. \quad (14)$$

Here results obtained by solving Eq. (11) for interchange modes in cylindrical stellarator plasmas with locally flattened pressure profiles [9] are briefly summarized: (i) The Suydam condition becomes irrelevant for examining the stability [15]. (ii) The radial mode structure near the marginal stability becomes similar to that of the  $m = 1$  internal kink mode near the rational surface and is extended to the inside ( $r < r_s$ ) or the outside ( $r > r_s$ ), where  $r_s$  is the radius of a rational surface. (iii) The marginal beta value for the low  $m$  mode resonant at  $r = r_s$  increases in relation to the Suydam limit [15]. (iv) It becomes easier to stabilize the higher harmonics with a narrower flat pressure region.

#### 4. Stabilization of low $n$ interchange modes with flat pressure regions at rational surfaces in toroidal plasmas

For the pressure profile given by Eq. (8) in the LHD model configuration, global pressure driven modes with  $n = 1, 2, 3$  are examined with the RESORM code [14], where  $n$  is the toroidal mode number.

##### 4.1. $n = 1$ mode

The smooth pressure profile  $P_0(\rho)$  and the rotational transform profile  $\iota(\rho)$  are plotted in Fig. 1. The rational surfaces for the  $n = 1$  mode,  $\iota = 1/1$  and  $\iota = 1/2$ , are shown by the dotted lines in the figure. Here the peak beta value is assumed to be 2%. The unstable  $n = 1$  mode exists with a growth rate of  $4.846 \times 10^{-2}$ ; it is destabilized at the  $\iota = 1/2$  surface. Here the growth rate is normalized by the poloidal Alfvén time. When the width  $w$  of the flat pressure region is increased at the  $\iota = 1/2$  surface, the growth rate decreases, as shown in Fig. 2. A marginally stable pressure profile against the  $n = 1$  mode with

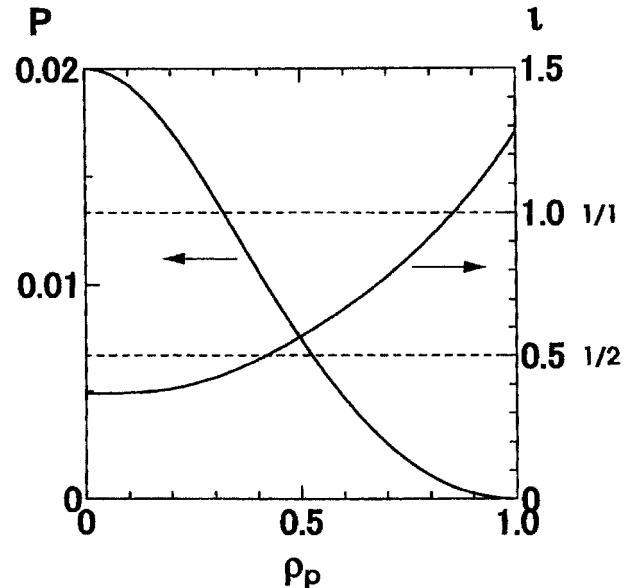


**Figure 1.** An assumed pressure profile and a rotational transform profile in the LHD configuration with an inward magnetic axis shift of 25 cm obtained with the VMEC code [13]. The dotted lines show  $\iota = 1/1$  and  $\iota = 1/2$ . The central beta value is  $\beta(0) = 2\%$  and the average beta value is  $\bar{\beta} = 0.632\%$ . The radius  $\rho_F$  denotes the square root of the normalized poloidal flux, which is also used in Figs 3–10.

$w = 0.045$  is shown in Fig. 3. For the weakly unstable  $n = 1$  mode with  $\gamma = 8.583 \times 10^{-3}$  in the case of  $w = 0.032$ , the radial mode structure of the stream function is shown in Fig. 4. Here the sharp decrease of  $u$  at the  $\iota = 1/2$  surface is as expected from the stability theory for the interchange mode in the cylindrical plasma model, as discussed in Section 2.

##### 4.2. $n = 2$ mode

Here the same pressure and rotational transform profiles as shown in Fig. 1 are used for the stability analysis of the  $n = 2$  mode. However, the number of the relevant rational surfaces increases:  $\iota = 2/2$ ,  $\iota = 2/3$ ,  $\iota = 2/4$  and  $\iota = 2/5$ . The RESORM code shows that the  $n = 2$  mode is destabilized at the rational surfaces  $\iota = 2/4$  and  $\iota = 2/5$ . Here the growth rate is  $\gamma = 7.187 \times 10^{-2}$  at  $\beta(0) = 2\%$ . Thus it is necessary to introduce two locally flat pressure regions with different widths at  $\iota = 2/4$  and  $\iota = 2/5$  for stabilizing the  $n = 2$  mode. When  $w = 0.02$  at  $\iota = 2/4$  and  $w = 0.04$  at  $\iota = 2/5$ , the instability is suppressed completely. The pressure profile obtained is shown in Fig. 5.

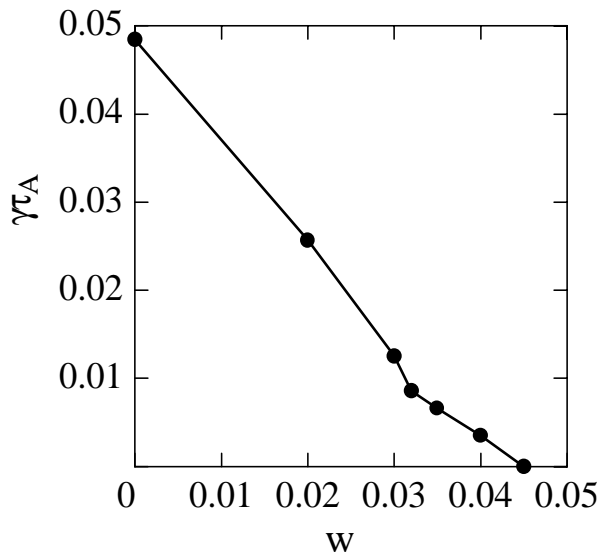


**Figure 2.** Growth rate of the  $n = 1$  pressure driven mode versus the width  $w$  of the flat pressure region at the  $\iota = 1/2$  surface. Here time is normalized by the poloidal Alfvén transit time.

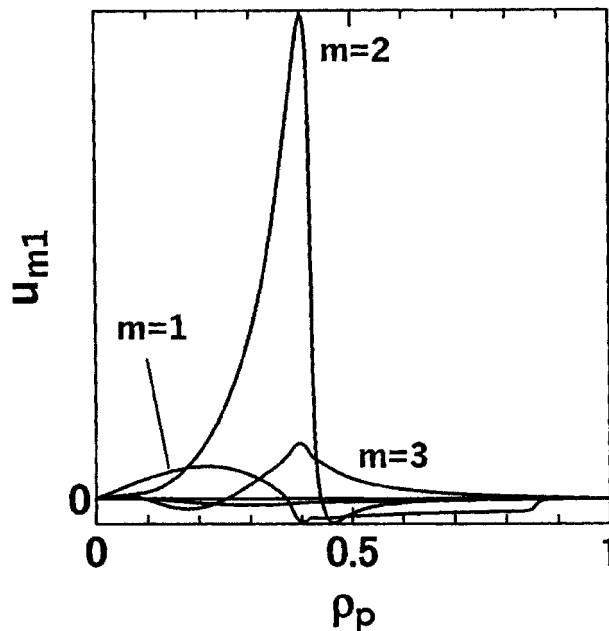


**Figure 4.** Radial mode structure of the stream function for  $w = 0.032$  at the  $\iota = 1/2$  surface. The growth rate is  $\gamma = 8.583 \times 10^{-3}$ .

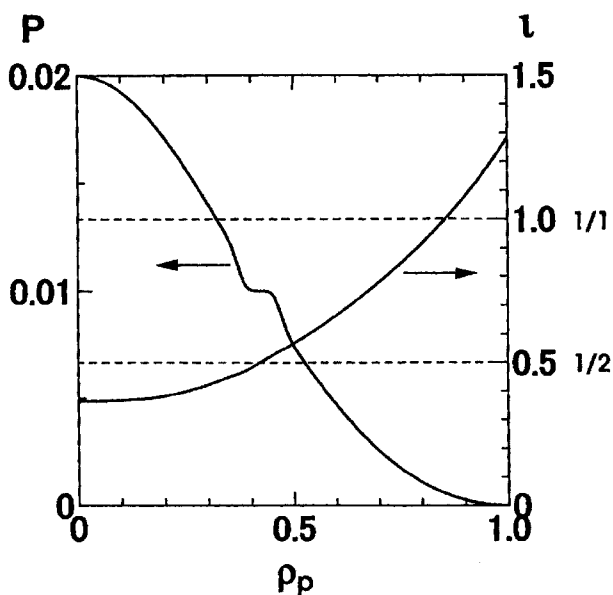


**Figure 3.** A marginally stable pressure profile against the  $n = 1$  pressure driven mode with the width of the flat pressure region  $w = 0.045$ . The rotational transform profile obtained with the VMEC code and rational surfaces  $\iota = 1/1$  and  $\iota = 1/2$  are also shown.

#### 4.3. $n = 3$ mode

For the LHD configuration with the pressure and rotational transform profiles shown in Fig. 1, there are six rational surfaces:  $\iota = 3/3, 3/4, 3/5, 3/6, 3/7$

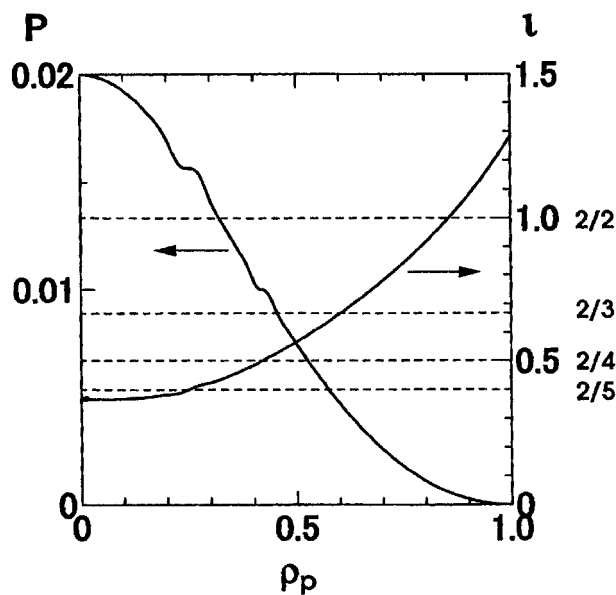


**Figure 5.** A marginally stable pressure profile against the  $n = 2$  pressure driven mode with the flat pressure regions given by  $w = 0.04$  at  $\iota = 2/5$  and  $w = 0.02$  at  $\iota = 2/4$ . The rotational transform profile obtained with the VMEC code and rational surfaces  $\iota = 2/2, 2/3, 2/4$  and  $2/5$  are shown.

and  $3/8$ . The RESORM code gives the growth rate  $\gamma = 8.233 \times 10^{-2}$  at  $\beta(0) = 2\%$ . The radial mode structure of the stream function is shown in Fig. 6.

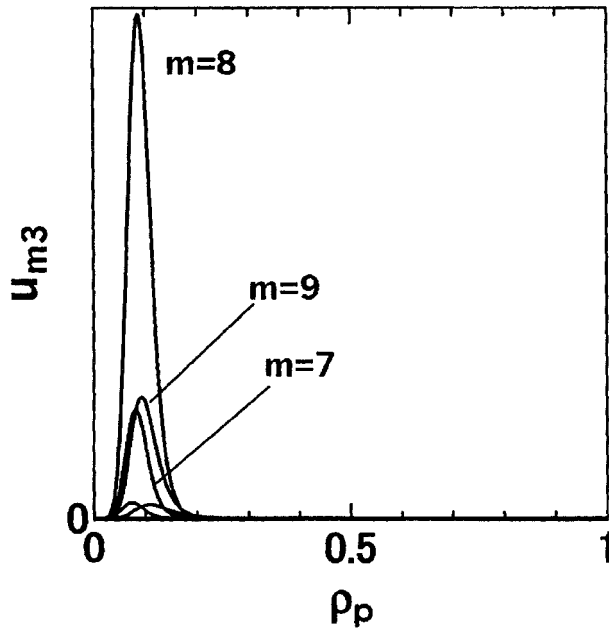


**Figure 6.** Radial mode structure of the stream function localized near the magnetic axis. The growth rate is  $\gamma = 8.233 \times 10^{-2}$  and the mode structure has ballooning mode characteristics.

Note that the unstable mode is localized at the central region with a ballooning structure. These are typical characteristics of the toroidal non-resonant pressure driven mode [16]. To suppress both this non-resonant mode and a resonant mode at  $\iota = 3/8$ , the central pressure profile is flattened first with  $w_a = 0.6$  in Eq. (9), as shown in Fig. 7. Then the growth rate decreases to  $\gamma = 6.975 \times 10^{-2}$ , and the unstable mode has a typical interchange mode structure destabilized at  $\iota = 3/4, 3/5, 3/6$  and  $3/7$ , as shown in Fig. 8. For suppressing the pressure driven interchange mode with  $n = 3$  completely, flat pressure regions are generated at the four rational surfaces with  $w = 0.03$  at  $\iota = 3/7$ ,  $w = 0.03$  at  $\iota = 3/6$ ,  $w = 0.02$  at  $\iota = 3/5$  and  $w = 0.02$  at  $\iota = 3/4$ . The pressure profile obtained with  $\beta(0) = 2\%$  is shown in Fig. 9. The average beta value is changed from  $\bar{\beta} = 0.632\%$  (Fig. 1) to  $\bar{\beta} = 1\%$  (Fig. 9).

It was demonstrated that the pressure driven modes with  $n = 1$ ,  $n = 2$  and  $n = 3$  can be stabilized by generating locally flat pressure regions at the relevant rational surfaces separately. Furthermore, it is confirmed that the  $n = 1, 2, 3$  modes become stable simultaneously when the pressure profile is described with  $w_a = 0.6$  and locally flat regions with  $w = 0.025, 0.03, 0.065, 0.03, 0.025$  and  $0.02$  at  $\iota = 0.4, 3/7, 0.5, 0.6, 2/3$  and  $0.75$ , respectively (Fig. 10).

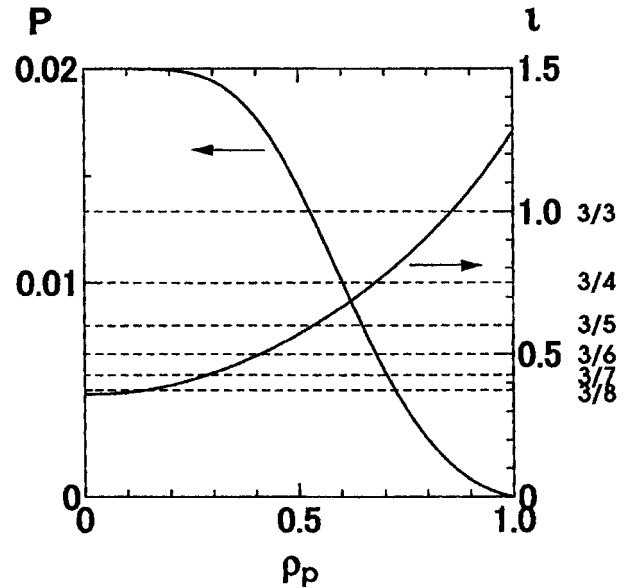


**Figure 7.** The central region of the pressure profile in Fig. 1 is flattened with the parameter  $w_a = 0.6$  in Eq. (15). The rotational transform profile obtained with the VMEC code and rational surfaces  $\iota = 3/3, 3/4, 3/5, 3/6, 3/7$  and  $3/8$  are shown.

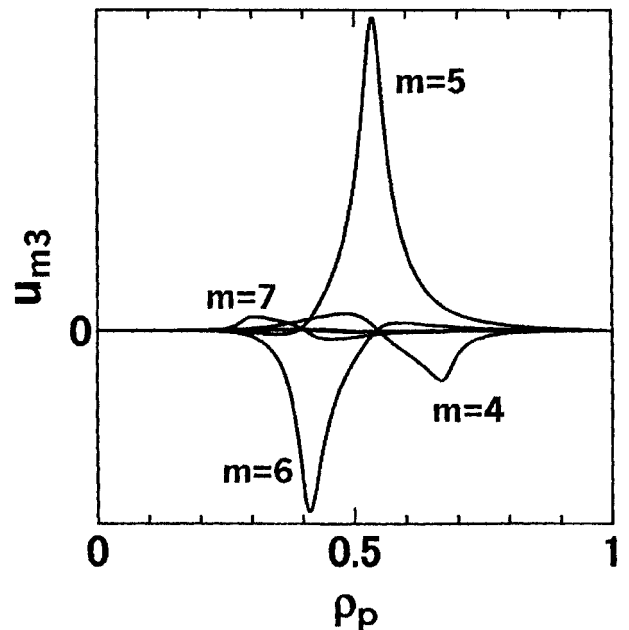


**Figure 8.** Radial mode structure of the stream function for the  $n = 3$  pressure driven mode with  $\gamma = 6.975 \times 10^{-2}$  after suppression of the non-resonant mode.

## 5. Concluding remarks

We have shown that pressure profiles with local flattening at the low order resonant surfaces lead to

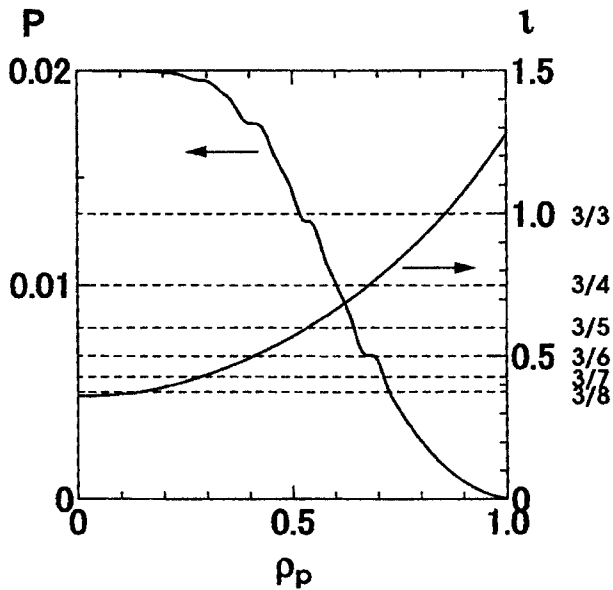


**Figure 9.** A marginally stable pressure profile against the  $n = 3$  pressure driven mode with the flat pressure regions given by  $w = 0.03$  at  $\iota = 3/7$ ,  $w = 0.03$  at  $\iota = 3/6$ ,  $w = 0.02$  at  $\iota = 3/5$  and  $w = 0.02$  at  $\iota = 3/4$ . The rotational transform profile obtained with the VMEC code and rational surfaces  $\iota = 3/3, 3/4, 3/5, 3/6, 3/7$  and  $3/8$  are shown.

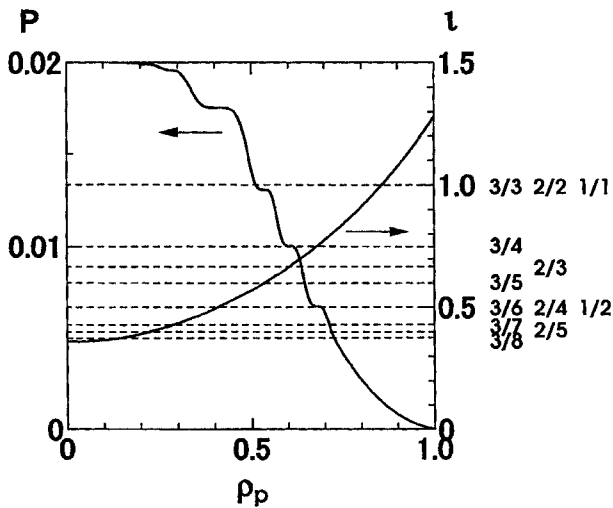


**Figure 10.** A marginally stable pressure profile against the pressure driven mode with  $n = 1, 2$  and  $3$  simultaneously. Here  $w = 0.025, 0.03, 0.065, 0.03, 0.025$  and  $0.02$  at  $\iota = 0.4, 3/7, 0.5, 0.6, 2/3$  and  $0.75$ , respectively.

higher stability limits for stellarator/heliotron configurations. This local flattening can be the spontaneous result of the non-linear evolution of resistive interchange modes that are unstable for values of beta well below the Mercier stability limit. In this

case, we should note that the size and degree of flattening might depend on dissipative effects such as resistivity and viscosity. However, there are other ways of creating such locally flat pressure profiles. One way is by externally applying resonant magnetic fields. In either situation, we have shown that the low  $n$  pressure driven instabilities are stabilized for the LHD model configurations. If the pressure gradient near the magnetic axis is large, non-resonant modes with toroidal mode numbers around 3 or 4 may also be destabilized. Therefore, to increase the ideal beta limits, broad pressure profiles with several flat spots in the low order resonant surfaces may be needed in LHD.

There is some evidence that experiments have exceeded the beta values given by the Mercier criterion when evaluated with smooth pressure profiles. For instance, there are observations of this type from CHS [17, 18] and Heliotron E [19]. The above mentioned existence of local flat spots at the low order rational surfaces may explain the discrepancy. The resistive interchange modes may be the mechanism causing these flat spots in the magnetic hill regions of those plasmas. Of course, there are other possible explanations for this discrepancy. Finite Larmor radius or kinetic effects may cause the stabilization of the large  $n$  modes. LHD has achieved plasmas with  $\bar{\beta} \simeq 2.4\%$ ; this value of beta appears to already exceed the Mercier limit calculated with a smooth pressure profile. More high  $\beta$  LHD experiments are needed to fully test our conjecture.

### Acknowledgement

This work was supported by a grant-in-aid from the Ministry of Education, Science, Sport and Culture (Monbusho), Japan.

### References

- [1] Motojima, O., et al., Phys. Plasmas **6** (1999) 1843.
- [2] Ohyabu, N., et al., Phys. Plasmas **7** (2000) 1802.
- [3] Yamada, H., et al., Phys. Rev. Lett. **84** (2000) 1216.
- [4] Sakakibara, S., et al., IAEA-CN-77/EXP3/12, paper presented at 18th IAEA Conf. on Fusion Energy, Sorrento, 2000.
- [5] Mercier, C., Nucl. Fusion **1** (1960) 47.
- [6] Wakatani, M., Stellarator and Heliotron Devices, Oxford Univ. Press (1998).
- [7] Hegna, C.C., Bhattacharjee, A., Phys. Fluids B **1** (1989) 392.
- [8] Nakamura, Y., et al., Phys. Fluids B **2** (1990) 2528.
- [9] Tatsuno, T., et al., Nucl. Fusion **39** (1999) 1391.

- [10] Ichiguchi, K., et al., J. Plasma Fusion Res. SERIES **2** (1999) 286.
- [11] Carreras, B.A., et al., Plasma Phys. Rep. **25** (1999) 958.
- [12] Strauss, H.R., Plasma Phys. **22** (1980) 2733.
- [13] Hirshman, S.P., et al., Comput. Phys. Commun. **43** (1986) 143.
- [14] Ichiguchi, K., et al., Nucl. Fusion **29** (1989) 2093.
- [15] Carreras, B.A., et al., IAEA-CN-77/THP2/3, paper presented at 18th IAEA Conf. on Fusion Energy, Sorrento, 2000.
- [16] Carreras, B.A., et al., Phys. Plasmas **5** (1998) 3700.
- [17] Okamura, S., et al., Nucl. Fusion **35** (1995) 283.
- [18] Okamura, S., et al., Nucl. Fusion **39** (1999) 1337.
- [19] Wakatani, M., et al., in Plasma Physics and Controlled Nuclear Fusion Research 1990 (Proc. 13th Int. Conf. Washington, DC, 1990), Vol. 2, IAEA, Vienna (1991) 567.

(Manuscript received 5 October 2000  
Final manuscript accepted 8 November 2000)

E-mail address of M. Wakatani:  
wakatani@energy.kyoto-u.ac.jp

Subject classification: C0, St